Published in final edited form as:
Graefes Arch Clin Exp Ophthalmol. 2013 January ; 251(1): 213–220. doi:10.1007/s00417-012-2052-2.

Unprocessed real-time imaging of vitreoretinal surgical maneuvers using a microscope-integrated spectral-domain optical coherence tomography system

Paul Hahn,
Department of Ophthalmology, Duke University Eye Center, Durham, NC 27710, USA

Justin Migacz,
Department of Biomedical Engineering, Duke University, Durham, NC 27708, USA

Rachelle O'Connell,
Department of Ophthalmology, Duke University Eye Center, Durham, NC 27710, USA

Joseph A. Izatt, and
Department of Ophthalmology, Duke University Eye Center, Durham, NC 27710, USA

Department of Biomedical Engineering, Duke University, Durham, NC 27708, USA

Cynthia A. Toth
Department of Ophthalmology, Duke University Eye Center, Durham, NC 27710, USA

Department of Biomedical Engineering, Duke University, Durham, NC 27708, USA

Cynthia A. Toth: cynthia.toth@duke.edu

Abstract

Background—We have recently developed a microscope-integrated spectral-domain optical coherence tomography (MIOCT) device towards intrasurgical cross-sectional imaging of surgical maneuvers. In this report, we explore the capability of MIOCT to acquire real-time video imaging of vitreoretinal surgical maneuvers without post-processing modifications.

Methods—Standard 3-port vitrectomy was performed in human during scheduled surgery as well as in cadaveric porcine eyes. MIOCT imaging of human subjects was performed in healthy normal volunteers and intraoperatively at a normal pause immediately following surgical manipulations, under an Institutional Review Board-approved protocol, with informed consent from all subjects. Video MIOCT imaging of live surgical manipulations was performed in cadaveric porcine eyes by carefully aligning B-scans with instrument orientation and movement. Inverted imaging was performed by lengthening of the reference arm to a position beyond the choroid.

Results—Unprocessed MIOCT imaging was successfully obtained in healthy human volunteers and in human patients undergoing surgery, with visualization of postsurgical changes in unprocessed single B-scans. Real-time, unprocessed MIOCT video imaging was successfully obtained in cadaveric porcine eyes during brushing of the retina with the Tano scraper, peeling of superficial retinal tissue with intraocular forceps, and separation of the posterior hyaloid face. Real-time inverted imaging enabled imaging without complex conjugate artifacts.

Correspondence to: Cynthia A. Toth, cynthia.toth@duke.edu.

Electronic supplementary material The online version of this article (doi:10.1007/s00417-012-2052-2) contains supplementary material, which is available to authorized users.

Conclusions—MIOCT is capable of unprocessed imaging of the macula in human patients undergoing surgery and of unprocessed, real-time, video imaging of surgical maneuvers in model eyes. These capabilities represent an important step towards development of MIOCT for efficient, real-time imaging of manipulations during human surgery.

Keywords

Optical coherence tomography; OCT; Intrasurgical; Intraoperative; Microscope-integrated; Vitreoretinal surgery; Unprocessed; Real-time

Introduction

Optical coherence tomography, with its ability to obtain high-resolution, cross-sectional retinal information quickly and non-invasively, has revolutionized clinical ophthalmologic practice. Recently, a handheld OCT has been developed to image patients unable to sit at a conventional tabletop scanner, including patients undergoing surgery in the operating room [1]. Intraoperative imaging with the handheld OCT has demonstrated relief of macular traction surrounding a macular hole after internal limiting membrane peel, removal of vitreo-macular adhesions following hyaloid peel, the presence of a deeper layer of epiretinal membrane following initial superficial membrane peel, and the persistence of subclinical subretinal fluid during retinal detachment repair [1–6].With the handheld OCT, surgical maneuvers are halted before imaging is initiated, and the handheld OCT is therefore unable to image live vitreoretinal surgical maneuvers.

Several groups are currently developing OCT towards intrasurgical imaging of live maneuvers [7]. Han et al. reported successful imaging of intraocular structures in cadaveric porcine eyes using a 21-G probe with an integrated OCT scanner [8]. Similarly, Balicki et al. have incorporated a single optical fiber interfaced to a custom SDOCT unit within a 25-G probe [9], which may be useful for intrasurgical imaging. Binder et al. reported imaging of 25 human retinas undergoing surgery using a Zeiss Cirrus SDOCT adapted to a surgical microscope [10]. Our group has also developed a custom microscope-integrated OCT (MIOCT), designed to fold the optical path of a spectral-domain OCT scanner into the optical path of a surgical microscope and thereby enable simultaneous surgical viewing and OCT acquisition [11, 12]. It is noteworthy that we have recently updated the nomenclature of our device, which we previously called microscope-mounted OCT (MMOCT), to MIOCT to reflect its true integration into the operating microscope.

In previous reports, we used MIOCT to provide the first OCT characterization of vitreoretinal surgical instruments interacting with the retina in a static fashion [12]. We have also demonstrated the ability of MIOCT to video image motion, capturing vitreoretinal surgical maneuvers in model eyes [13]. Our previous imaging was generally limited by the need for significant post-processing modifications, reducing its applicability for real-time use that requires instantaneous output. In this report, we present the ability of MIOCT to image surgical maneuvers in human patients undergoing surgery and to acquire real-time, unprocessed video imaging of several vitreoretinal surgical maneuvers using MIOCT in model eyes.

Methods

MIOCT design

As previously described, a microscope-integrated spectral-domain optical coherence tomography (MIOCT) prototype device was developed to interface optically and mechanically with a Leica (Wetzlar, Germany) operating microscope [11]. The design

allowed folding of the optical path of the MIOCT into that of the surgical microscope in order to permit simultaneous imaging during surgical manipulations without altering the surgeon's view. This prototype used a superluminescent diode illumination source with a center wavelength of 840 nm, a 49-nm full-width at half maximum bandwidth, and a spectrometer equipped to acquire at a rate of 20,000 A-scans per second. The signal sensitivity was 112 dB at an illumination power of 700 μW. The axial and lateral resolutions in the eye were 5 μm and 15 μm respectively. The field of view was 10 mm wide, and the depth range was 2.24 mm.

Imaging of human subjects outside of and during vitreoretinal surgery

The Duke University Institutional Review Board and Data and Safety Monitoring Committee approval for a research protocol in accordance with all applicable Health Insurance Portability and Accountability Act regulations was obtained, along with informed consent from all human patients undergoing MIOCT imaging. Human fundus imaging was performed using the MIOCT with <700 μW illumination power at the pupil. Human MIOCT imaging was performed through the Binocular Indirect Ophthalmo-Microscope (BIOM) wide-angle viewing system (Oculus Inc., Lynnwood, WA, USA) first in healthy, non-surgical subjects imaged in the supine position to simulate conditions during surgery, and then in surgical subjects during standard 3-port vitrectomy and macular surgery performed by a single surgeon (C.A.T.). MIOCT images were acquired as 6- or 8-mm linear scans with 1,000 A-scans per B-scan, using Bioptigen v1.6 software to operate the device, to orient acquired B-scans, and to obtain raw data from the scans (Bioptigen, Research Triangle Park, NC, USA). Imaging in surgical patients was performed at a normal pause following surgical manipulations with instruments removed from the eye.

Intraoperative simulation with model eyes

Standard 3-port vitrectomy was performed in fresh cadaveric porcine eyes. With visualization under an MIOCT-mounted Leica surgical microscope, a 19-gauge MVR blade was used to create three sclerotomies. An infusion line was placed through one sclerotomy to maintain consistent intraocular pressure. A fiberoptic light for endoillumination and a vitreoretinal surgical instrument were placed through the remaining sclerotomies. Retinal structures were visualized either through a disposable flat contact lens (Dutch Ophthalmic, Exeter, NH) or through the BIOM wide-angle viewing system. Instruments included the Tano diamond-dusted membrane scraper (Synergetics, O'Fallon, MO, USA), the vitreous cutter (Alcon, Fort Worth, TX, USA), and intraocular forceps (Alcon).

Model eye intraoperative imaging protocol

Using the MIOCT device to obtain B-scans, Bioptigen v1.6 software was employed to operate the device, to orient acquired B-scans, and to obtain raw data from the scans. Scans were carefully oriented in cadaveric eyes to image perpendicular to or along the longitudinal axis of instruments. All movements were also directed either perpendicular to or along the axis of the instrument. The reference arm and the BIOM focus, when applicable, were adjusted to optimize image quality for all scan sets. Cadaveric porcine images through the flat contact lens were obtained with 4-mm serial B-scans containing 1,000 A-scans per B-scan. Cadaveric images through the BIOM were obtained with 5-mm serial B-scans containing 500 A-scans per B-scan. No post-processing algorithms of video scan sets in cadaveric porcine eyes were applied.

Inverted imaging

To obtain images with the inverted imaging technique, the reference arm length was increased to reposition the zero delay position from its typical position anterior to the retina

to a new location posterior to the retina. The live image was then flipped in the software in order to correct the orientation. As above, BIOM focus and reference arm length were adjusted to optimize image quality.

Results

In order to demonstrate optimal performance of the MIOCT system for cadaveric porcine retinal imaging, an initial set of static images was obtained prior to video imaging of motion. These static images, acquired as a Tano diamond-dusted membrane scraper lay against a cadaveric porcine eye, were post-processed by co-registering and averaging 20 frames for improved signal-to-noise ratio and speckle reduction. MIOCT was successfully able to demonstrate in three dimensions the Tano scraper interacting with the retinal surface (Fig. 1). These cadaveric eyes exhibit visible retinal opacification, and individual retinal layers are not identified, even on post-processed OCT imaging.

Human imaging of normal human volunteers (Fig. 2a) was performed to confirm that poor identification of retinal layers was due to post mortem tissue degradation and not a deficiency in resolution of the MIOCT. A single, unprocessed B-scan through a healthy fovea demonstrates a resolution comparable to unprocessed images from SDOCT tabletop scanners, with identification of all retinal layers including multiple hyperreflective bands in the outer retina. This high resolution indicates feasibility of unprocessed imaging during human surgery and further confirms that post mortem tissue degradation contributes significantly to loss of MMOCT resolution in cadaveric eyes.

Human MIOCT imaging of a patient undergoing vitrectomy for vitreomacular traction with subretinal fluid (Fig. 2b,c) was then performed with acquisition of OCT images at a normal pause following surgical maneuvers. Immediately following surgical separation of the posterior hyaloid and peeling of the internal limiting membrane, an edge of peeled internal limiting membrane is visualized. On the unprocessed, single B-scan, speckle artifact partially obscures clear identification of all retinal layers, but the inner retinal surface and retinal pigment epithelium (RPE)–outer retinal complex can be clearly identified. Subretinal fluid, present pre-operatively, is noted at the fovea with inner retinal elevation. As expected, postprocess averaging and registration of 12 frames reduces speckle and improves resolution. The flap of peeled internal limiting membrane is observed, and the extent of subretinal fluid with inner retinal elevation is clearly delineated.

Following static imaging of surgical maneuvers, MIOCT was then assessed for its ability to image movements in cadaveric porcine eyes with real-time, unprocessed videorate serial B-scans. Careful alignment of B-scan orientation with the perpendicular or longitudinal axis of the surgical instrument was required for effective video imaging of linear movements. Imaging was successfully performed through the disposable flat contact lens and through the non-contact BIOM wide-angle viewing system.

B-scans oriented perpendicular to the tip of the Tano diamond-dusted membrane scraper demonstrate the instrument in motion brushing against the cadaveric porcine retinal surface (Fig. 3, Supplemental Videos 1, 2). Significant inward deflection of the inner retinal surface can be observed, which is induced by pressure from the membrane scraper (Fig. 3a–d, Supplemental Video 1). Lighter brushing with the instrument (Fig. 3e–h, Supplemental Video 2) results in visibly less deflection of the inner retina. The diamond-dusted instrument tip exhibits hyper-reflectivity with diminished visibility of underlying retinal structures, as we have previously reported [12]. Clear identification of distinct retinal layers is not possible in these cadaveric eyes, in contrast to the MIOCT retinal images obtained with the same system in normal human volunteers and human surgical participants.

Orientation of B-scans along the long axis of the Tano scraper also enabled effective imaging of longitudinal movement of the instrument in porcine eyes (Fig. 4, Supplemental Videos 3, 4). As noted, retinal visibility under the hyper-reflective diamond-dusted tip is limited. There is also complete shadowing under the metallic instrument shaft. Posterior reflection of the shaft of the instrument at the zero delay position forms a complex conjugate artifact (Fig. 4a–d, Supplemental Video 3), which can be removed by an inverted imaging technique performed by lengthening of the reference arm prior to imaging (Fig. 4e–h, Supplemental Video 4). Inverted imaging does not remove shadowing, and complete shadowing under the shaft is still observed after elimination of the complex conjugate artifact.

Surgical changes in tissue morphology can also be observed in cadaveric eyes with unprocessed serial B-scans. A flap of inner retinal tissue pre-formed with a barbed MVR blade can be observed as it is peeled with intraocular forceps along the axis of the scan (Fig. 5, Supplemental Video 5). Complete shadowing is observed under the metallic forceps. Improved viewability is obtained with the dynamic views afforded by video imaging (Supplemental Video 5) compared to static imaging with isolated frames (Fig. 5). As with other scans obtained in cadaveric eyes, post mortem tissue degradation prevents identification of distinct retinal structures on OCT imaging.

In addition to imaging instrument–retina interactions, intrasurgical MIOCT may also be useful in identifying changes in retinal morphology induced by distant surgical maneuvers. Imaging of the cadaveric porcine retina during surgically-induced separation of the posterior hyaloid face reveals an outwardly progressing ridge of subtle retinal elevation as the faintly visible overlying vitreous is separated from the retinal surface (Fig. 6, Supplemental Video 6). This ridge may correspond to a shifting micro-detachment of the retina, which appears to promptly reattach as the vitreous separation progresses.

Discussion

We have recently developed a microscope-integrated spectral-domain OCT system to enable real-time intrasurgical imaging of vitreoretinal surgical maneuvers [11]. Using this system, we have previously reported successful imaging of vitreoretinal surgical manipulations in cadaveric porcine eyes [13], but this imaging generally required significant post-processing modifications for adequate viewability. As microscope-integrated OCT systems are further developed towards real-time imaging of vitreoretinal surgical procedures in humans, efficiency and real-time viewability will be critical. Instantaneous post-processing modifications will need to be incorporated into the OCT-driving software, or ideally, images will be successfully obtained without the need for post-processing methods.

In this report, we present the ability of our MIOCT system to image normal human volunteer subjects and human subjects undergoing vitreoretinal surgery. The resolution of images obtained intraoperatively was lower than those obtained in healthy volunteers. There may be subclinical corneal or other media opacities related to surgery that cause degradation of image quality. Despite this difference in resolution, post-surgical changes, including a flap of peeled internal limiting membrane, can be clearly visualized in both unprocessed single-frame MIOCT imaging and in summed frames at a normal pause immediately following surgical manipulations. Similarly, in another microscope-integrated OCT system, based on a Zeiss Cirrus SDOCT unit mounted onto a Zeiss surgical microscope, visibility of unprocessed images acquired in human patients undergoing surgery was improved by post-processing modifications [10].

We additionally present the first demonstration of unprocessed, real-time video imaging of several common vitreoretinal surgical manipulations in model eyes using MIOCT. Without the need for any post-processing modifications, we were able to successfully image the Tano membrane scraper brushing against the retinal surface with B-scans oriented both perpendicular to the tip and along the instrument shaft. We were also able to successfully image changes in tissue morphology as intraocular forceps peeled a flap of superficial retinal tissue. And we were able to successfully image a shifting microdetachment of the retina corresponding to surgically-induced separation of the overlying vitreous. Our ability to obtain real-time, unprocessed videos using the MIOCT is an important progression of MIOCT towards efficient imaging with real-time applicability.

We also demonstrate use of an inverted imaging technique to remove complex conjugate artifacts. This technique involves lengthening of the reference arm to shift the zero delay position below the retina, rather than above, which is typically performed for retinal imaging. These adjustments are similar to the adjustments optimized for imaging the choroid, including enhanced depth imaging employed by the Heidelberg Spectralis SDOCT system [14]. Our inverted imaging technique applied in MIOCT similarly improves visibility of the choroid and other deep structures and removes the complex conjugate artifact, while still permitting real-time video imaging without the need for post-processing modifications. This technique may prove useful in select circumstances.

Significant shadowing exists below the surgical instruments. We have previously reported on the use of spatial compounding, a post-processing modification, to interpolate retinal information from adjacent B-scans as a means of artificially removing this shadowing artifact [13]. Real-time removal of this shadowing artifact would require instantaneous post-processing algorithms, such as the spatial compounding algorithm, to be incorporated into the OCT software. Alternatively, novel instrumentation constructed of materials with improved transmission properties may improve visibility of the underlying retina, and current efforts are underway to develop such instruments.

Our ability to obtain images efficiently is currently limited by the careful alignment required to position the OCT beam appropriately in relation to the area of interest and the direction of motion. We are currently developing tracking options that would allow the MIOCT to target a continually moving area of interest, such as the instrument tip, in an automated and instantaneous fashion. In this report, we have shown the ability of MIOCT to image movements both perpendicular to and along the axis of surgical instruments, suggesting that with tracking, we will able to image movements in all directions.

The time currently required for alignment of scan direction with instrument orientation is not practical during human surgery. Without tracking, the use of microscope-integrated OCT systems in human surgery may be limited to imaging of a relatively fixed region. Tracking options would reduce or even eliminate the need for manual alignment currently required for successful imaging, and will be critical to enable rapid visualization of active surgical manipulations. In this report, we demonstrate that real-time, unprocessed video imaging is feasible in model eyes, predicting that incorporation of tracking into the MIOCT device may be the final significant hurdle towards efficient real-time intrasurgical MIOCT imaging in human surgery.

Conclusion

We demonstrate the ability of MIOCT to capture real-time, unprocessed video imaging of motion during various vitreoretinal surgical maneuvers. We also demonstrate the ability of MIOCT to acquire high-resolution, unprocessed human images. Compared to post-processed

video imaging, the ability to produce these unprocessed video images of surgical maneuvers represents a significant advance and proof-of-principle of MIOCT as it is developed towards seamless and efficient imaging of human patients undergoing surgery.

Supplementary Material

Refer to Web version on PubMed Central for supplementary material.

Acknowledgments

The authors would like to acknowledge Katrina Winters and Michelle McCall for their administrative assistance, along with Tomas Moreno and Eric Yuan for their technical assistance.

Supported by the Heed Ophthalmic Foundation (PH), NIH: 1UL1 RR024128-01; 1R21 EY019411

Dr. Toth receives research support through equipment loan from Bioptigen, and has potential for royalties for OCT-related technology licensed by Duke to Bioptigen. Dr. Toth also receives royalties for surgical technology licensed by Duke to Alcon Laboratories. Duke University has an equity interest in Bioptigen.

Dr. Izatt is a co-founder of Bioptigen, Inc., and has corporate, intellectual property, and equity interests in this company.

References

1. Dayani PN, Maldonado R, Farsiu S, Toth CA. Intraoperative use of handheld spectral-domain optical coherence tomography imaging in macular surgery. Retina. 2009; 29:1457–1468. [PubMed: 19823107]
2. Baranano DE, Fortun JA, Ray R, Charkoudian L, Bergstrom C, Cribbs B, Schwent B, Hubbard G, Srivastava S. Intraoperative spectral-domain optical coherence tomography for macular pucker surgery. ARVO Meeting Abstracts. 2010; 51:269.
3. Lee LB, Srivastava SK. Intraoperative spectral-domain optical coherence tomography during complex retinal detachment repair. Ophthalmic Surg Lasers Imaging 42 Online. 2011:e71–e74.
4. Ray R, Baranano DE, Fortun JA, Schwent BJ, Cribbs BE, Bergstrom CS, Hubbard GB 3rd, Srivastava SK. Intraoperative microscope-mounted spectral-domain optical coherence tomography for evaluation of retinal anatomy during macular surgery. Ophthalmology. 2011; 118:2212–2217. [PubMed: 21906815]
5. Wykoff CC, Berrocal AM, Schefler AC, Uhlhorn SR, Ruggeri M, Hess D. Intraoperative OCT of a full-thickness macular hole before and after internal limiting membrane peeling. Ophthalmic Surg Lasers Imaging. 2010; 41:7–11. [PubMed: 20128563]
6. Scott AW, Farsiu S, Enyedi LB, Wallace DK, Toth CA. Imaging the infant retina with a hand-held spectral-domain optical coherence tomography device. Am J Ophthalmol. 2009; 147(364–373):e362.
7. Hahn P, Migacz J, O'Connell R, Maldonado R, Izatt JA, Toth CA. The use of optical coherence tomography in intraoperative ophthalmic imaging. Ophthalmic Surg Lasers Imaging. 2011; 42:S85–S94. [PubMed: 21790116]
8. Han S, Sarunic MV, Wu J, Humayun M, Yang C. Handheld forward-imaging needle endoscope for ophthalmic optical coherence tomography inspection. J Biomed Opt. 2008; 13:020505. [PubMed: 18465947]
9. Balicki M, Han JH, Iordachita I, Gehlbach P, Handa J, Taylor R, Kang J. Single fiber optical coherence tomography microsurgical instruments for computer and robot-assisted retinal surgery. Med Image Comput Comput Assist Interv. 2009; 12:108–115. [PubMed: 20425977]
10. Binder S, Falkner-Radler CI, Hauger C, Matz H, Glittenberg C. Feasibility of Intrasurgical spectral-domain optical coherence tomography. Retina. 2011; 31:1332–1336. [PubMed: 21273942]
11. Tao YK, Ehlers JP, Toth CA, Izatt JA. Intraoperative spectral-domain optical coherence tomography for vitreoretinal surgery. Opt Lett. 2010; 35:3315–3317. [PubMed: 20967051]

12. Ehlers JP, Tao YK, Farsiu S, Maldonado R, Izatt JA, Toth CA. Integration of a spectral-domain optical coherence tomography system into a surgical microscope for intraoperative imaging. Invest Ophthalmol Vis Sci. 2011; 52:3153–3159. [PubMed: 21282565]
13. Tao YK, Ehlers JP, Toth CA, Izatt JA. Visualization of vitreoretinal surgical manipulations using intraoperative spectraldomain optical coherence tomography. Proc SPIE. 2011; 7889:78890F.
14. Spaide RF, Koizumi H, Pozzoni MC. Enhanced depth imaging spectral-domain optical coherence tomography. Am J Ophthalmol. 2008; 146:496–500. [PubMed: 18639219]

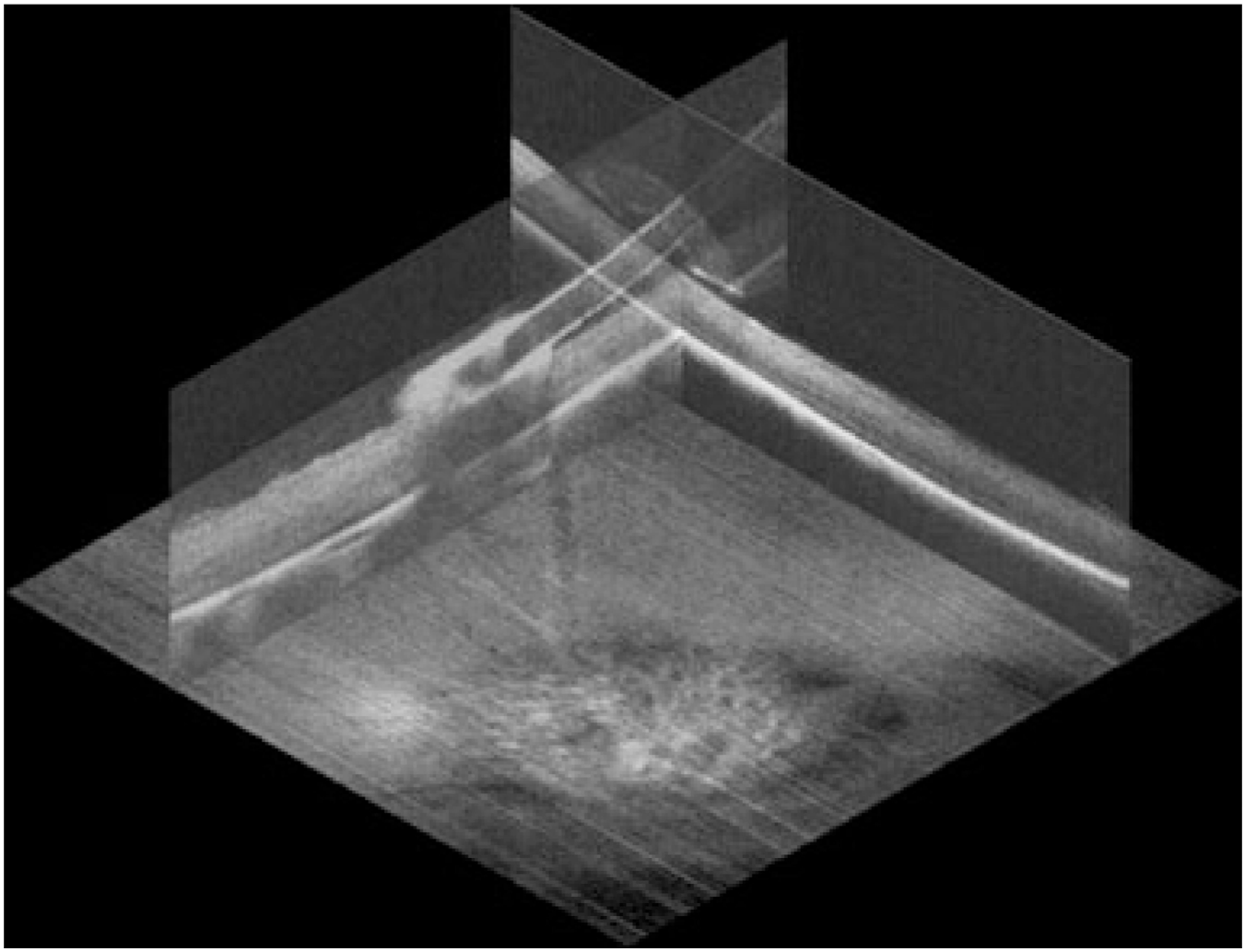

Fig. 1.
Three-dimensional static rendering of Tano diamond-dusted membrane scraper brushing against a cadaveric porcine retina. Summed and averaged orthogonal MIOCT B-scans obtained through a flat contact lens are oriented over the corresponding summed voxel projection

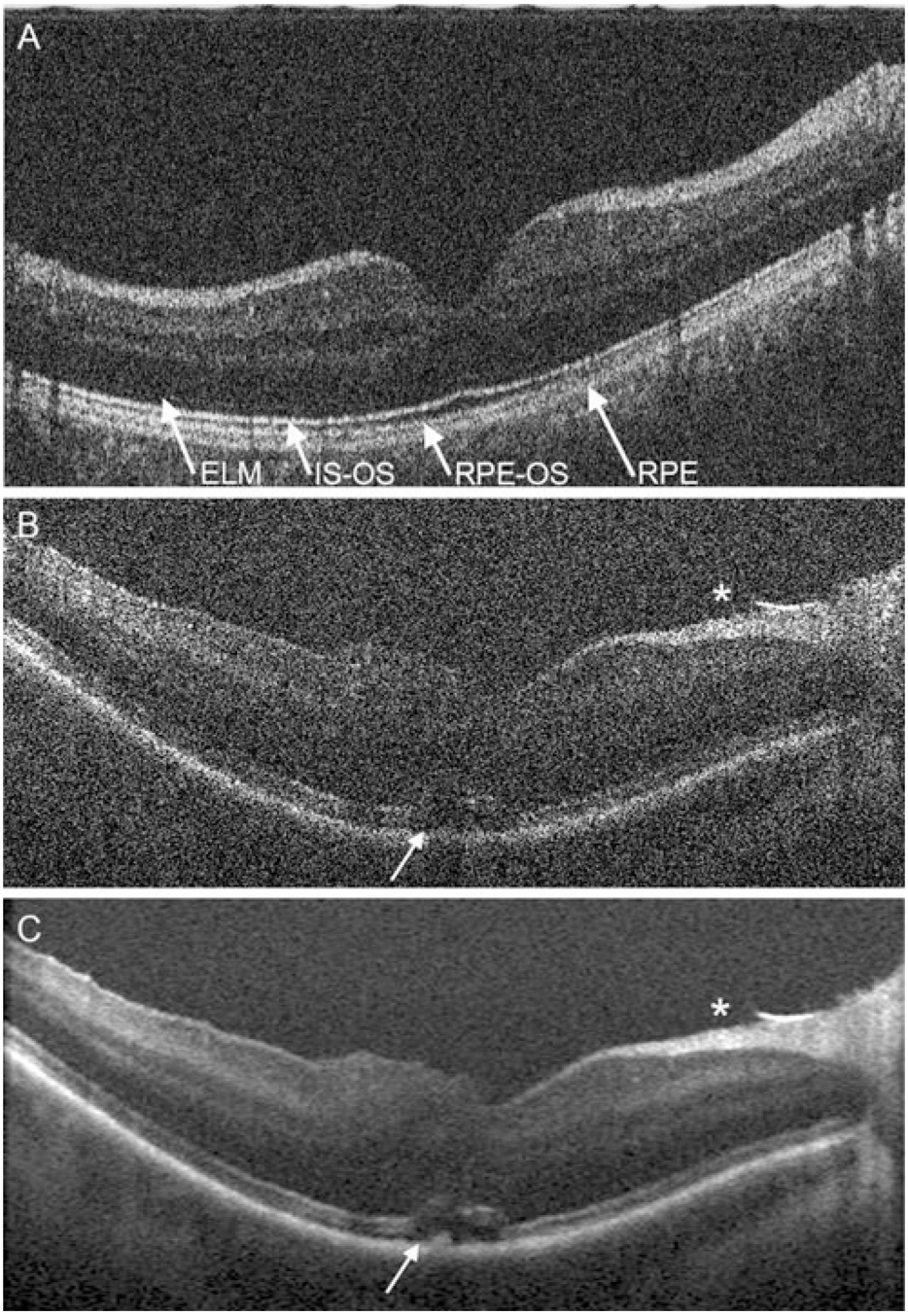

Fig. 2.

MIOCT B-scans acquired through the non-contact BIOM from a healthy human volunteer (**a**) and from a human patient undergoing surgery at a normal pause immediately following surgical maneuvers (**b,c**). A single, unprocessed B-scan from a healthy human volunteer demonstrates resolution of individual retinal layers (**a**). Multiple outer retinal bands can be resolved, corresponding to the external limiting membrane (*ELM*), inner segment–outer segment junction (*IS-OS*), retinal pigment epithelium–outer segment junction (*RPE-OS*), and retinal pigment epithelium (*RPE*). Following surgical hyaloid separation and internal limiting membrane peel for vitreomacular traction, a single unprocessed B-scan (**b**)

demonstrates a free edge of peeled internal limiting membrane (*) along with persistence of unchanged subretinal fluid (*arrow*) and inner retinal elevation, which are visualized with higher resolution and less speckle artifact on the processed image (**c**)

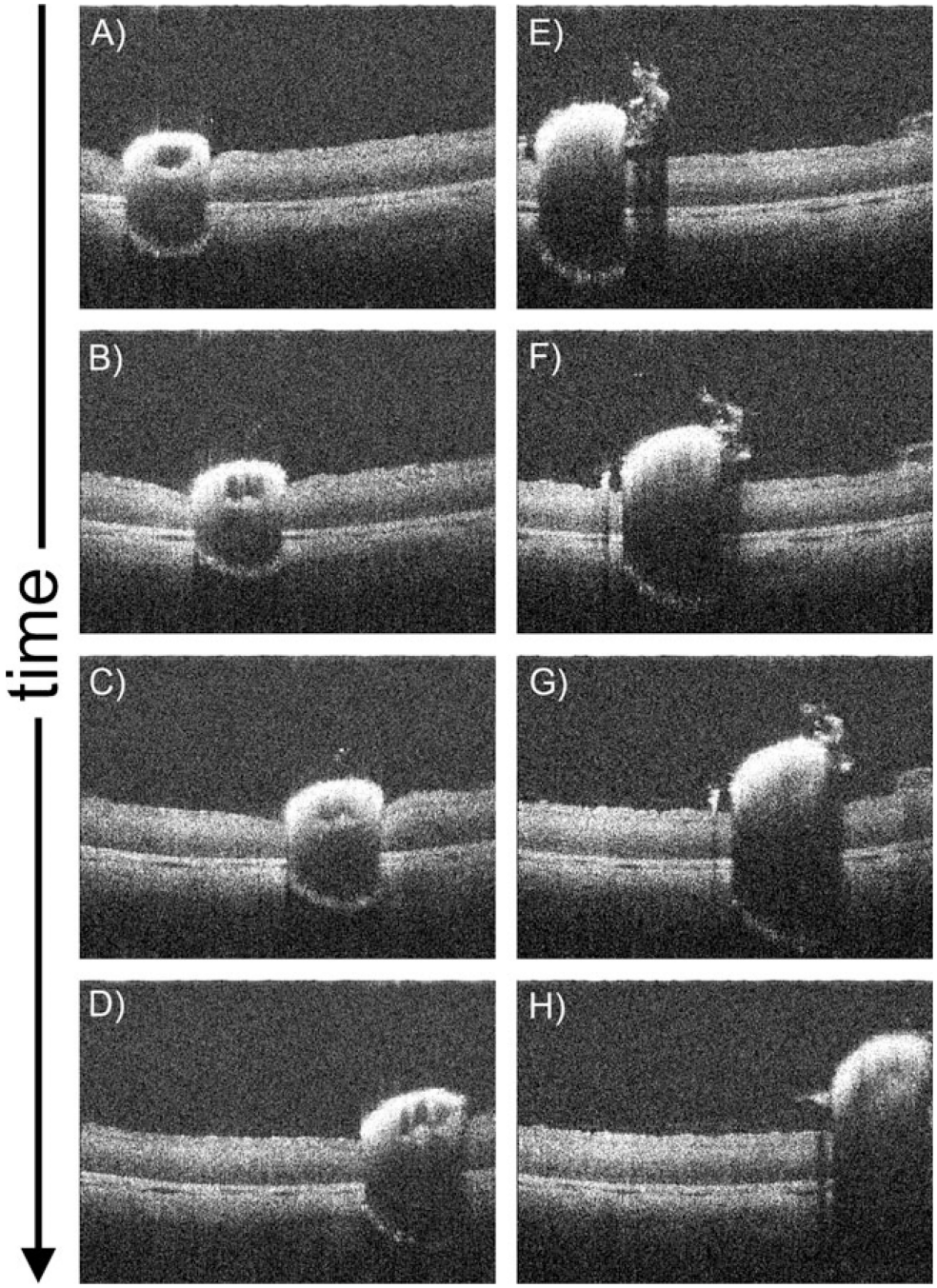

Fig. 3.

Single MIOCT B-scan frames from real-time unprocessed video imaging oriented perpendicular to a Tano diamond-dusted membrane scraper brushing against the retinal surface of a cadaveric porcine eye. These images were obtained through a flat contact lens. Significant inward deflection of the inner retinal surface can be observed (**a–d**; Supplemental Video 1), which is decreased with less intense brushing (**e–h**; Supplemental Video 2)

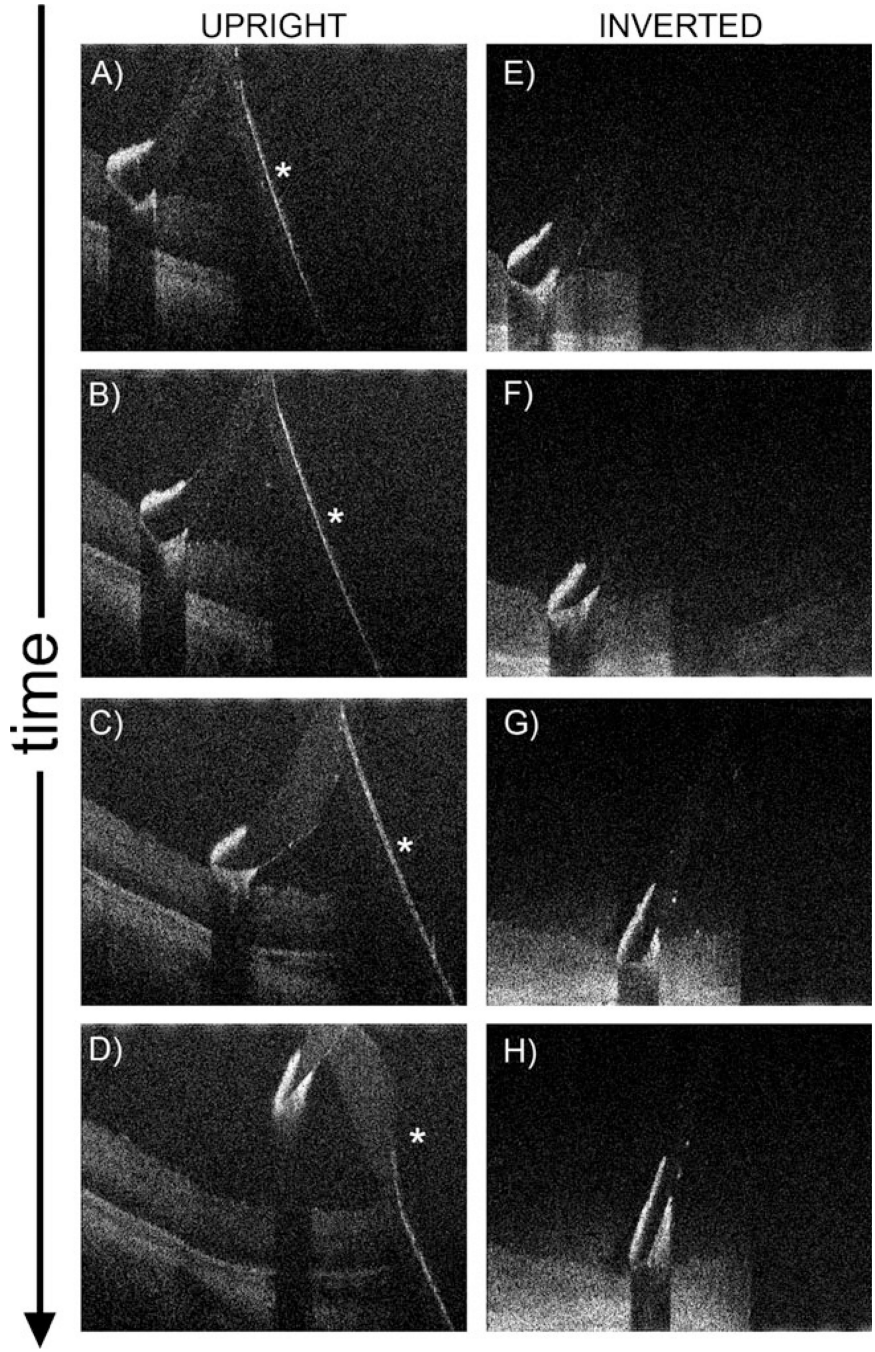

Fig. 4.

Single MIOCT B-scan frames from real-time unprocessed video imaging oriented along the longitudinal axis of the Tano diamond-dusted membrane scraper brushing against the retinal surface of a cadaveric porcine eye. These images were obtained through the non-contact BIOM. A reflection of the shaft of the instrument, which is a complex conjugate artifact (*asterisk*), is observed (**a–d**; Supplemental Video 3). This artifact can be removed using an inverted imaging technique (**e–h**; Supplemental Video 4)

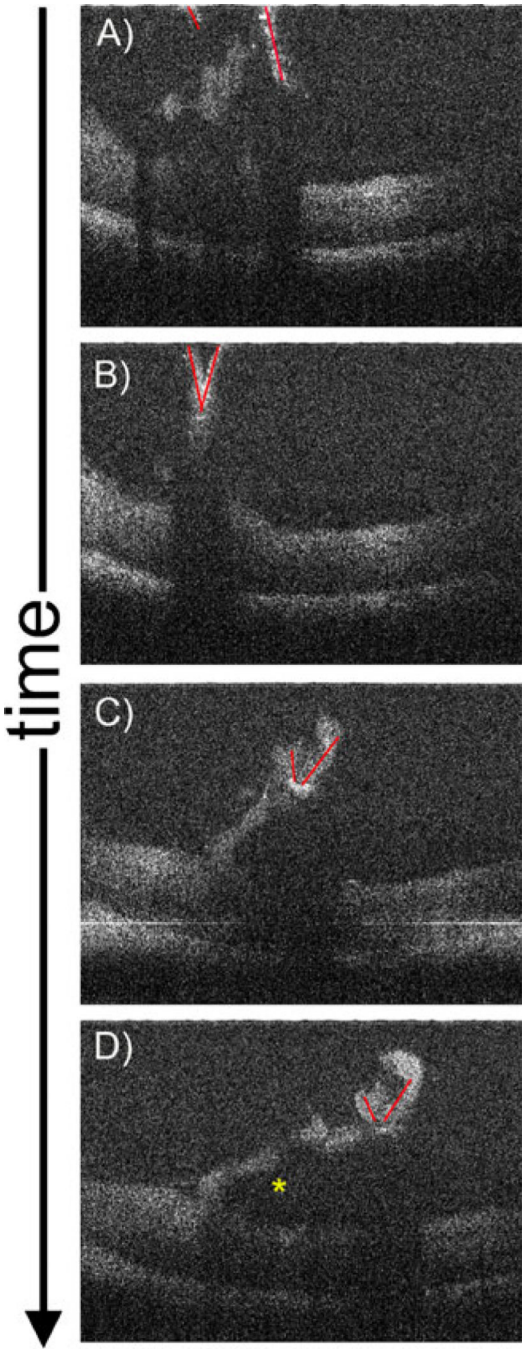

Fig. 5.
Single MIOCT B-scan frames from real-time unprocessed video imaging (Supplemental Video 5) demonstrating intraocular forceps (highlighted with *red lines*) grasping and peeling a flap of cadaveric porcine superficial retinal tissue. These images were obtained through a flat contact lens. The retinal flap was created with a barbed MVR blade prior to imaging (not shown). The forceps can be seen peeling the flap to the right of the images, until the flap breaks free (*asterisk*)

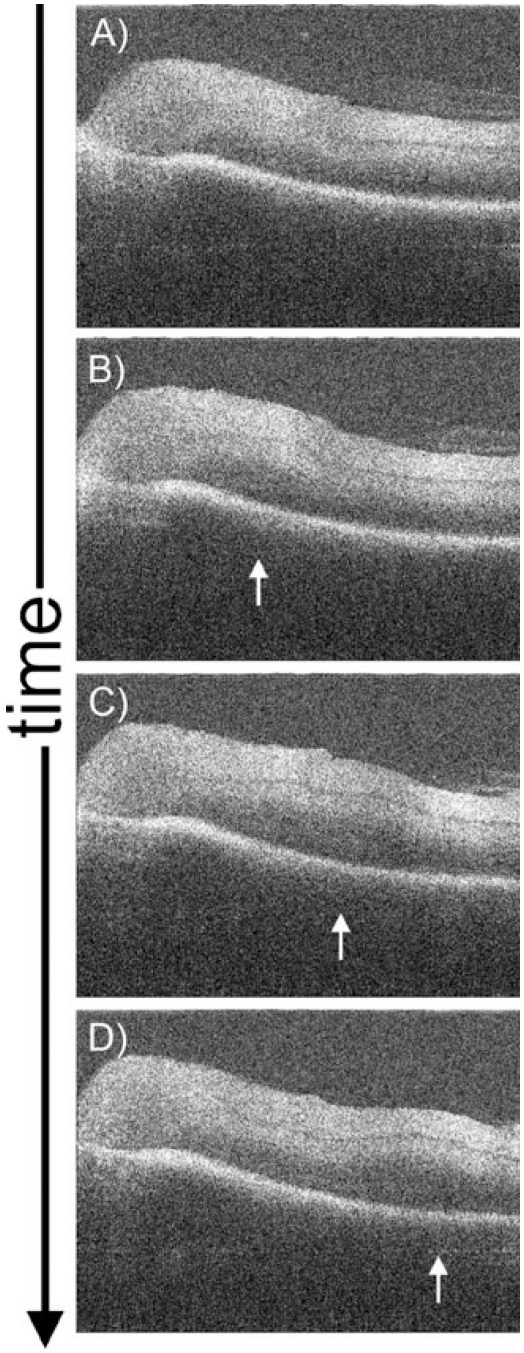

Fig. 6.

Single MIOCT B-scan frames from real-time unprocessed video imaging (Supplemental Video 6) demonstrating retinal changes during surgical separation of the posterior hyaloid face in a cadaveric porcine eye. These images were obtained through a flat contact lens. In this series, the vitreous cutter (not seen) placed over the optic nerve head was used to aspirate and engage the posterior hyaloid, which was then elevated anteriorly, resulting in a circumferentially spreading separation of the vitreous from its attachments to the retina. As the vitreous separates, a corresponding ridge of outwardly progressing retinal elevation (*arrows*) is observed